Chapter 5
Ultrathin Oxide Films on Au(111) Substrates

Chen Wu and Martin R. Castell

Abstract The Au(111) surface is an excellent substrate for the growth of ultrathin oxide films. Although it is chemically relatively inert, the high electronegativity of Au tends to give rise to strong interactions between the oxide film and the substrate via charge transfer processes. Many new surface oxide structures with unique properties have been observed in ultrathin film form that have no analogues as bulk crystal terminations.

Abbreviations

2D	Two-dimensional
3D	Three-dimensional
AES	Auger electron spectroscopy
CVD	Chemical vapor deposition
FCC	Face centered cubic
HCP	Hexagonal close packing
LEED	Low-energy electron diffraction
MBE	Molecular beam epitaxy
ML	Monolayer
PVD	Physical vapor deposition
RHEED	Reflection high energy electron diffraction
RLAD	Reactive-layer-assisted deposition
RT	Room temperature
SMSI	Strong metal-support interactions
STM	Scanning tunneling microscopy
STS	Scanning tunneling spectroscopy

C. Wu (✉)
School of Materials Science and Engineering, State Key Laboratory of Silicon Materials, Zhejiang University, 310027 Hangzhou, China
e-mail: chen_wu@zju.edu.cn

M.R. Castell (✉)
Department of Materials, University of Oxford, Parks Road, Oxford OX1 3PH, UK
e-mail: martin.castell@materials.ox.ac.uk

F.P. Netzer and A. Fortunelli (eds.), *Oxide Materials at the Two-Dimensional Limit*, Springer Series in Materials Science 234, DOI 10.1007/978-3-319-28332-6_5

TMAA	Trimethyl acetic acid
TPD	Thermal programmed desorption
UHV	Ultrahigh vacuum
XPS	X-ray photoelectron spectroscopy

5.1 Introduction

Ultrathin oxide films consist of only a few monolayers (MLs) of oxide material with a typical thickness ranging between 1 and 2 nm. They are of extensive interest in the context of new technologies and fundamental research. Oxide ultrathin films can be incorporated into various advanced technologies including plasma display panels, microelectronic devices and metal-oxide catalysts [1–3]. For these applications, ultrathin films provide novel properties, decreased component size for device miniaturization, and significantly increased surface-to-volume ratios for enhanced catalytic performance.

One of the difficulties in the study of native oxide surfaces is that many of them are electrically insulating, and therefore do not lend themselves to be characterized with electron-based probes such as X-ray photoelectron spectroscopy (XPS), scanning tunneling microscopy (STM), or low-energy electron diffraction (LEED). However, this problem can be circumvented through the growth of very thin oxide films on metal substrates. Oxide thin films also provide model surfaces, since a much wider range of oxides can be grown in the form of thin layers than are available as bulk crystals [4]. Ultrathin films can have novel surface structures which do not correspond to the thermodynamically favored terminations of bulk crystals [5]. For example, polar planes of some bulk oxides have been considered to be unstable since the repeat unit of the stacking sequence perpendicular to the surface has a non-zero dipole moment. Alternating cationic and anionic layers of the bulk crystal leads to an infinite surface energy. The polarity is usually compensated by various surface mechanisms including substoichiometry, reconstruction and molecular adsorption [6]. However, in principle, a stoichiometric and unreconstructed polar surface can be achieved in ultrathin films because there is no macroscopic dipole. New structures of ultrathin films also arise due to the strong template effect of the substrate, which opens up the opportunity for fabricating a broad variety of epitaxial oxide materials with novel physical and chemical properties.

Noble metal crystal surfaces serve as an important type of substrate for ultrathin oxide film growth due to their relatively simple preparation procedures, chemical stability, and high electrical conductivity that eliminates charging effects. Oxides grown on metal substrates can be considered as inverse models for catalytic oxide-supported metal nanoparticles. The complexity of real-world catalyst materials tend to hinder in-depth investigations of their active sites and reaction mechanisms. However, inverse model catalysts with ordered oxide structures deposited on metal substrates allow for the exploration of some fundamental steps in

heterogeneous catalysis using a variety of surface science tools. An oxide/metal system that has attracted much attention is that of oxide-supported Au nanoparticles which acts as an excellent catalysts in the conversion of CO into CO_2 at remarkably low temperatures (200 K) [7, 8]. Another important area is the catalytic activity of the Au/oxide systems towards the water-gas shift reaction ($H_2O + CO \rightarrow H_2 + CO_2$) [9, 10]. Au catalysts supported on a variety of oxides are also active for many other reactions such as NO reduction, selective oxidation of propene to propene oxide and the production of ethyl acetate from ethanol, etc. [11–13]. The unique catalytic properties of oxide-supported Au catalysts have also stimulated extensive studies into inverse model catalysts that consist of oxide thin films supported on Au single crystal substrates, and recent research indicates that such inverse systems are catalytically active themselves. Excellent performance has been reported for CeO_x and TiO_x nanoparticles grown on Au(111) with respect to the water-gas shift reaction [14, 15]. A further example is CO oxidation promoted by Fe_2O_3 or TiO_2 nanoclusters grown on Au(111) [16, 17]. The catalytic activity for both Au/oxide and oxide/Au systems has stimulated research into the Au-oxide interaction. To gain a better understanding of this system, the growth of oxide thin films on Au(111) can provide some valuable insights.

5.2 Preparation and Characterization Methods

5.2.1 Thin Film Growth

The growth of oxide ultrathin films on noble metal substrates usually involves evaporation of the component materials onto the substrate. Since the oxide generally possesses a higher sublimation temperature than the corresponding metal, thermal evaporation of the metal is often carried out either from an electron-beam evaporator or an effusion cell. The evaporation is sometimes carried out in an oxidizing atmosphere. An alternative method is to evaporate the metal in UHV and then post-anneal the sample in an oxidizing gas environment using, for example O_2 or NO_2. This latter method tends to be the most widely-used process for the formation of oxide thin films [18–22]. The oxidation process may vary for different methods, e.g. in reactive-layer-assisted deposition (RLAD), Ti is evaporated onto a Au(111) substrate pre-deposited with a layer of H_2O or N_2O and post-annealing then gives rise to TiO_x structures [23, 24]. RLAD has also been reported for the CeO_x/Au(111) system where a pre-deposited H_2O or NO_2 layer was used [25]. Oxidation of an alloy substrate such as Ti–Au has also been reported in the preparation of TiO_2 crystallites on Au(111) [26]. Recently, chemical vapor deposition (CVD) has been used to sublime gaseous titanium tetrasopropoxide. The Ti $(OC_3H_7)_4$ precursor decomposes on the Au(111) substrate and forms an ultrathin TiO_x film [27]. CVD has also been used to deposit Mo clusters using $Mo(CO)_6$ as a precursor followed by oxidation in NO_2 to form MoO_3 on Au(111) [28].

5.2.2 Thin Film Characterization

The conductive nature of the Au substrate allows various surface characterization techniques to be used that involve electrons, enabling in-depth investigation of the ultrathin films. Classical techniques for surface structure determination involve electron diffraction at different energies. Both LEED and reflection high energy electron diffraction (RHEED) provide convenient ways to determine the crystallinity and periodicity of the oxide films. Atomically resolved surface structure images can be obtained by STM. Meanwhile, scanning tunneling spectroscopy (STS) provides information on the local electronic properties of the films. Apart from structural investigations, determination of the chemical composition of the film is often also necessary. Electron-based spectroscopy including XPS, Auger electron spectroscopy (AES) and ultra-violet photoelectron spectroscopy (UPS) are surface sensitive, and are extremely useful in understanding the chemistry of the oxide films and the substrate-film charge transfer [29]. Theoretical analysis of proposed atomic models and prediction of the electronic structure can be carried out using density function theory (DFT). DFT is also used for calculation of the charge transfer at the substrate-film interfaces and the work function of the films.

5.3 Structural Features of the Oxide Films

5.3.1 The Au(111) Substrate Reconstruction

The nature of the substrate surface plays an important role in the determination of the film structure. The surface atoms of the clean substrate metal are not usually located in the positions of a simple bulk termination. This is because the atoms on the surface have a lower coordination number compared with those in the bulk [30]. The surface relaxes or reconstructs to minimize the surface free energy. Relaxation involves a subtle adjustment of the layer spacings perpendicular to the surface, but the periodicity or the symmetry parallel to the surface remains unchanged. A reconstruction refers to the rearrangement of the surface atoms to form a structure that differs from the bulk crystallographic planes.

Unreconstructed Au(111) planes consist of hexagonal lattices, as Au has a face centered cubic (fcc) crystal structure. For the reconstructed Au(111) surface, a complex structure consisting of paired rows is observed, as shown in the STM images in Fig. 5.1. The bright lines are boundaries between unfaulted fcc and faulted hexagonal close packed (hcp) stacking [31]. This faulting arises because the surface atomic bonds undergo a uniaxial contraction by 4 % along the $\langle 1\bar{1}0\rangle$ direction and the surface therefore contains more atoms than a bulk (111) plane. For every 22 atoms along the $\langle 1\bar{1}0\rangle$ direction in the bulk there are 23 surface atoms, resulting in a $(22 \times \sqrt{3})$ unit cell. This reconstruction is also sometimes erroneously called the $(23 \times \sqrt{3})$ reconstruction because of the 23 atoms in the surface

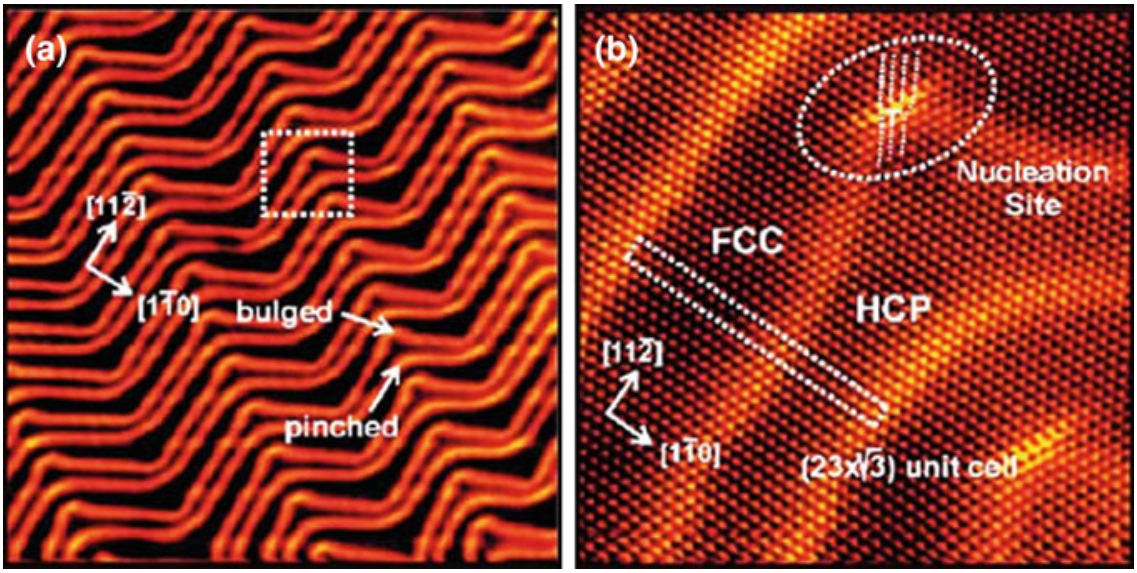

Fig. 5.1 STM images showing **a** large scale herringbone reconstruction of the Au(111) surface (Image size: 80.2 × 79.5 nm^2) and **b** atomically resolved $(22 \times \sqrt{3})$ unit cells on Au(111) (Image size: 14.1 × 13.5 nm^2; V_s = −0.04 V; I_t = 1.55 nA) [32, 33]

layer, however reconstructions should always refer to the bulk crystallography, and hence $(22 \times \sqrt{3})$ is the correct expression. Long-range forces on this surface further complicate matters in which the lowest energy configuration involves a periodic change in the direction of the reconstruction, and this results in a zig-zag appearance that is called the herringbone reconstruction.

5.3.2 *Structure of the Oxide Films*

A variety of oxide thin films have been fabricated on the Au(111) surface including TiO_x [18, 23, 24, 27], FeO_x [22, 34], VO_x [35–38], CoO [39–41], MoO_3 [28, 42, 43], MgO [19, 44–46], CeO_x [25], ZnO [47] and BaO_x [48]. The growth of ultrathin oxide films on the Au(111) surface usually lifts the herringbone reconstruction due to the strong interaction between the film and the substrate. This effect has been observed in various systems including TiO_x/Au(111) and MoO_3/Au(111) [18, 27, 49]. For cases where there is less than a monolayer coverage of the oxide, the herringbone lines wind around the oxide islands without going underneath them. This indicates that by forming the oxide-Au interface there is no longer an energetic advantage in compressing the top layer of Au atoms that results in the herringbone reconstruction and therefore the original Au(111) hexagonal lattice forms the template for film growth.

The phases obtained for the oxide films mainly include honeycomb, pinwheel, hexagonal, and row-like structures. The structure of the initial oxide monolayer of the film is strongly affected by the hexagonal symmetry of the Au(111) substrate. For the TiO_x/Au(111) system, STM reveals the co-existence of a honeycomb structure and a pinwheel structure as shown in Fig. 5.2 [18, 27]. The honeycomb

structure is formed with the Ti atoms occupying the three-fold hollow sites of the Au lattice and the O atoms located at the bridge sites of the Ti atoms, resulting in a stoichiometry of Ti_2O_3. The unit cell of the honeycomb structure aligns with the crystallographic directions of the Au substrate and corresponds to a (2 × 2) reconstruction. The pinwheel structure consists of six interlocking triangles. The atoms at the spokes occupy the Au bridge sites instead of the three-fold hollow sites of the lattice underneath. Consequently they are higher and appear brighter than the atoms within the triangles (Fig. 5.2b). The pinwheel structure originates from a Moiré pattern formed through the superposition of a metal/O lattice over the Au (111) surface [18]. The metal/O lattice is rotated by a certain angle with respect to the Au(111) lattice. Depending on the angle of rotation (whether clockwise or anticlockwise), two domains can be obtained for the pinwheel structure as shown in Fig. 5.2b. Two types of periodicities are observed by STM for the pinwheels: the unit cells by connecting the coincident points for the two lattices (Fig. 5.2b) and the atomic periodicity of the overlayer (Fig. 5.2c). The formation of the Moiré patterns may also lead to other appearances of the surface structure depending on the angle of rotation between the film and the substrate lattice. The most commonly observed Moiré patterns exhibit a hexagonal shape such as FeO(111) [34], CoO(111) [39, 41] and ZnO(0001) [47, 50] films on Au(111).

A hexagonal lattice has also been found for V_2O_3(0001)/Au(111) (Fig. 5.3), and for a number of years there were conflicting views concerning the detailed atomic structure of the film [51, 52]. While XPS and STM suggested a surface terminated with a vanadyl (V=O) group [37, 53], ion scattering investigations and ion beam triangulation supported the reconstructed O_3 model [35, 36, 38]. More recently, this controversy on the V_2O_3(0001) termination has been revisited and resolved via a

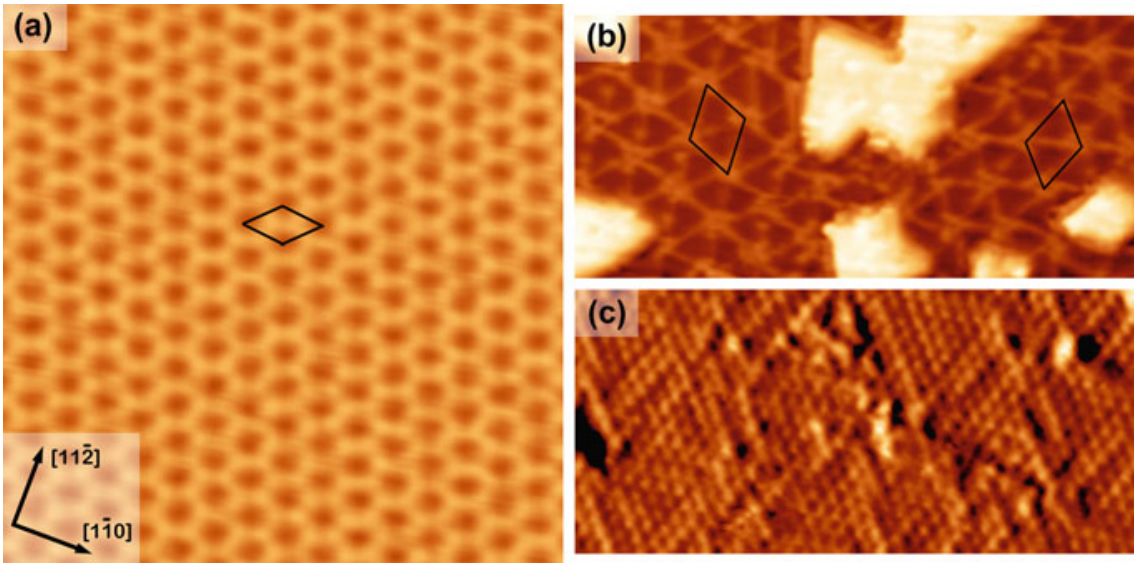

Fig. 5.2 STM images showing **a** the (2 × 2) honeycomb Ti_2O_3 structure on Au(111) (Image size: 8.5 × 8.5 nm^2; V_s = 0.98 V; I_t = 0.2 nA), **b** the pinwheel TiO monolayer with two domains indicated (Image size: 31 × 14 nm^2; V_s = 1.41 V; I_t = 0.18 nA) and **c** atomically resolved pinwheel structure on Au(111) (Image size: 11 × 5 nm^2; V_s = −0.12 V; I_t = 0.5 nA) [18]

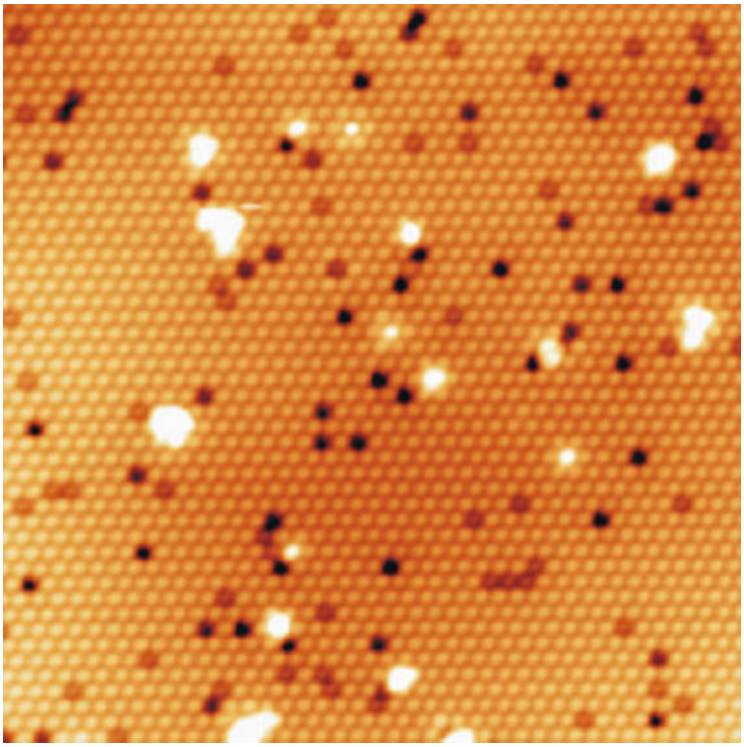

Fig. 5.3 STM image showing the $V_2O_3(0001)$ surface on an Au(111) substrate (Image size: 20×20 nm^2; $V_s = -1.5$ V; $I_t = 0.2$ nA) [52]

combination of I-V LEED, STM, fast atom scattering and DFT, indicating that the vanadyl termination is thermodynamically more stable [54]. It has also been reported that electron irradiation removes the O-involved termination, resulting in a vanadium terminated surface with three-fold symmetry and higher catalytic reactivity [55].

Other structures of vanadium oxide on Au(111) include $V_2O_5(001)$ and $V_6O_{13}(001)$ which exhibit row structures with rectangular or rectangular-like unit cells as shown in Fig. 5.4 [20, 21]. The $V_6O_{13}(001)$ phase grows as a double-layered film after completing the first layer of the $V_2O_5(001)$ structure. Both phases do not exist as a bulk termination and it is interesting that the second layer does not adopt the same unit cell as the first layer, demonstrating the significant influence of the Au (111) substrate on the structure of the first layer.

Monolayer MgO islands with both hexagonal (111) and rectangular-like (001) lattices exist on the Au(111) substrate depending on the deposition temperature and oxygen partial pressure [19, 44, 45]. The MgO(001) monolayer adopts a (6×1) superlattice with a stripe pattern, while triangular islands are seen for MgO (111) ultrathin films. Detailed total-energy calculations suggests that the MgO islands adopt the square lattice configuration with the perimeter formed by nonpolar [100] edges, while the MgO(111) islands are stabilized by hydroxylated polar zigzag edges [44, 46]. Different edges of the two types of oxide islands may be linked to molecular adsorption behavior and determine the catalytic reactivity. In the MoO_3/Au(111) system, the first monolayer of MoO_3 on Au(111) exhibits a c (4×2) structure [43, 49]. Increasing the Mo coverage gives rise to a bilayer MoO_3 film with a 11.6 Å × 5 Å rectangular unit cell. Beyond the bilayer structure,

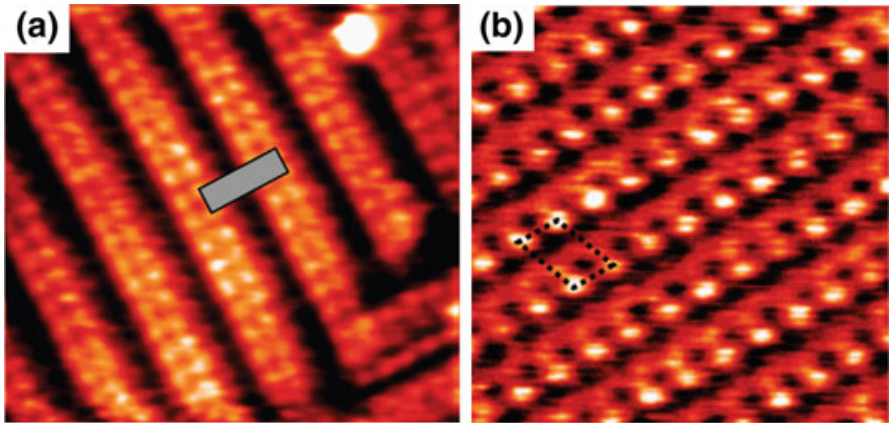

Fig. 5.4 STM images of **a** a V_2O_5 monolayer (Image size: 6.3 × 5.8 nm^2; V_s = 2 V; I_t = 0.2 nA) and **b** a V_6O_{13} ultrathin film (Image size: 3.4 × 3.4 nm^2; V_s = 2 V; I_t = 0.2 nA) on Au(111) prepared by oxidation of deposited vanadium [20, 21]

MoO_3(010) crystallites grow as the Mo dose is further increased, similar to the case of V_2O_5(001) on Au(111) [21].

The observed structures of ultrathin oxide films grown on Au(111) can be roughly divided into two categories. In the first category the structures possess three-fold symmetry, which can be attributed to the strong interaction between the film and the substrate lattice. The second category structures exhibit a stripe-pattern with rectangular (-like) unit cells. There are multiple reasons for the formation of these different phases, such as film stoichiometry, film thickness, and growth and processing conditions. These factors are discussed in turn in the following sections.

5.3.3 Structural Transitions of the Oxide Films

There are a number of factors that determine the growth behavior of ultrathin films, including the substrate-film lattice mismatch, the surface and interfacial energy of the system, the stoichiometry and thickness of the film, and the growth conditions of the oxide. These factors can interact with each other, making an understanding of the growth behavior even more challenging. Here we focus on the individual factors that can be manipulated in order to shed some light on how to influence the structure of oxide ultrathin films on Au(111).

5.3.3.1 Stoichiometry-Driven Structural Transitions

A significant variation of the chemical composition of a film inevitably leads to a change in its atomic structure. This is most easily achieved with metal elements that have multiple oxidation states, in which case the stoichiometry drives the formation of different structures of the oxide film. For example, for the first TiO_x monolayer grown on Au(111), a stoichiometry of Ti_2O_3 is obtained for the honeycomb

structure, whereas the pinwheel pattern corresponds to a stoichiometry of TiO [18, 56]. Another example are the rather different stoichiometry-driven phases observed for V_2O_3 (hexagonal), V_2O_5 (rectangular) and V_6O_{13} (rectangular-like) on Au(111) [20, 21, 35–38]. A change in the stoichiometry can be achieved by varying the growth conditions including the growth temperature, oxidation species, oxygen pressure and post-annealing process. For example, it has been found that increasing the growth temperature from 200 to 500 °C gives rise to preferential growth of 3D TiO_2 nanocrystals with rectangular unit cells rather than the 2D (2 × 2) honeycomb Ti_2O_3 lattice [27]. The oxidation method also plays an important role in the film stoichiometry. Ce metal nanoparticles on Au have limited reactivity toward molecular O_2 and NO_2 due to the formation of Ce–Au alloys, resulting in the formation of substoichiometric 3D CeO_x particles. Complete oxidation can be achieved by Ce deposition on to the Au substrate at elevated temperatures in an O_2 background pressure. This gives rise to ultrathin flat and ordered CeO_2(111) nanoislands with a hexagonal surface structure [25]. For the FeO_x/Au(111) system, oxidation of Fe deposited on Au(111) with molecular O_2 at room temperature (RT) gives rise to the growth of an FeO monolayer, while the Fe_2O_3 phase forms by oxidation with NO_2 at elevated temperatures [22, 34]. STM images reveal a hexagonal Moiré pattern for the FeO(111) phase and an O-terminated α-Fe_2O_3(0001) surface for the Fe_2O_3 phase. The oxygen pressure is also an important factor in the control of the stoichiometry of ultrathin oxide films on Au(111). It has been reported that Pb deposited on Au oxidizes to form PbO in an oxygen pressure (P_{O2}) less than 10^{-6} Torr. Increasing the P_{O2} to 10^{-4} Torr leads to the transition from PbO to PbO_2 [57]. Also, the ultrathin lead oxide film can be oxidized or reduced reversibly by thermal oxidation or vacuum annealing cycles. Similar effects of post-annealing on the stoichiometry have also been found for the CoO_x/Au(111) system [41] where the transition between the 2D CoO phase and the 3D Co_3O_4 phase can be tuned by oxidation and reduction annealing.

5.3.3.2 Lattice Mismatch-Driven Structural Transition

The degree of lattice mismatch between the film and substrate partially determines whether a wetting film with an ordered surface structure can be obtained. On the one hand, the lattice mismatch can be optimized by choosing an appropriate combination of oxide film and substrate to allow epitaxial growth to occur. On the other hand, a large lattice mismatch between the film and the substrate may be overcome by the formation of completely different structures from the bulk for the ultrathin films. For example, hexagonal Moiré patterns arise for the ZnO (0001)/Au (111) system due to the large lattice mismatch (approx. 12 %) [47]. The lattice mismatch may also give rise to the formation of different structures by varying the growth conditions. For MgO on Au(111), hexagonal symmetry arises with low temperature and O_2 partial pressure. MgO(001) with a stripe pattern forms with a higher temperature and oxygen pressure due to the symmetry mismatch of the square overlayer and the hexagonal substrate [19].

The influence of the lattice mismatch becomes weaker as the film grows thicker. For the TiO_x/Au(111) system, triangular islands start to grow as the second monolayer instead of the honeycomb Ti_2O_3 and pinwheel TiO wetting layer [18]. It is difficult to reveal the atomic structure of the second layer due to limited resolution of the STM images. One can however, infer that the second ML is still affected by the lattice of the Au(111) substrate because it nucleates as bright triangular islands that have inherited the three-fold symmetry of the substrate. Further increased Ti coverage results in the formation of a row structure on the triangular islands with a rectangular unit cell [18, 27], indicating a weakened influence of the substrate. Similarly, transitions between 2D Moiré-patterned CoO and 3D Co_3O_4 spinel clusters on Au(111) have also been reported by controlling the Co coverage [39, 41]. The strain introduced in the film by the substrate-film lattice mismatch can be relaxed with increased film thickness due to the introduction of crystal defects including point defects and misfit dislocations. Beyond a certain thickness the oxide film will tend to adopt its bulk structure. For example, a bulk-like CoO layer has been obtained for a coverage of 7 MLs on Au(111) [40]. This may even give rise to a different crystal orientation of the thicker film compared to the substrate in order to minimize the overall energy of the system. However, we will not discuss this phenomenon further in this chapter as it is devoted only to ultrathin films of thicknesses less than a few monolayers. A comprehensive understanding the influence of the film-substrate interaction, film stoichiometry and coverage on the stability of different oxide structures can be used to influence the oxide phase.

5.4 Interactions Between the Film and the Substrate

Apart from epitaxial effects of the substrate, interactions between the oxide ultrathin films and the substrate mainly consist of mass transport and charge redistribution [29]. In some instances ultrahigh vacuum (UHV) annealing of an Au substrate with a metal (M) deposited on it may lead to the formation of an M–Au alloy [25] in which case the oxide film can be grown by oxidation of the metal (M) extracted from the alloy [26]. The film-substrate mass exchange is usually neglected once the oxide has been formed due to the chemically inert nature of the Au substrate. The interfacial structure, however, needs to be considered for the first monolayer of the film on Au(111). Whether the oxide film starts with a densely packed layer of O or with one of the metal (M) atoms results in the different stacking sequences of Au–O–M or Au–M–O. The bonding energetics between Au and O or M need to be considered for the interfacial structure. Formation of M–Au alloys, the weak adsorption of O on Au and the fact that Au oxide easily decomposes indicate that Au prefers to bond with the metal (M) atoms, resulting in most cases in an Au–M–O interface [18, 40, 58].

Another important factor to consider for the film-substrate interactions is the charge transfer which is driven by the minimization of the system energy and the continuity of the electric potential in the solid [59]. For example, interfacial charge transfer between the oxide film and the electronegative gold surface, results in a

decreased work function of Au(111) following deposition of a MgO(001) monolayer [19]. A change in the work function is determined by the electronegativity of the substrate. A large decrease in work function has been reported for MgO/Au(111) compared with MgO/Mo(001) and MgO/Ag(001), indicating that Au substrates can be responsible for significant charge transfer between the adsorbates and the substrate [60]. For MgO/Au(111), DFT calculations indicate that the charge transfer compensates the polarity of the film [61]. Conversely, changes of the opposite sign can be induced in the work function of the substrate depending on the metal-oxide interface [60]. While MgO thin films decrease the substrate work function, growth of SiO_2 and TiO_2 films lead to raised work functions of the substrates. Consequently, a change in the work function of the substrate can be tuned by an appropriate choice of the metal-oxide interface. This can be explained by the electronegativity of the substrate which determines the sign and extent of the charge transfer at the metal-oxide interface [62]. These effects will be further discussed in the following section. Charge transfer is common for oxide-Au interfaces and has been reported for a number of systems including V_2O_3/Au(111) [53] and MoO_3/Au(111) [49, 63].

5.5 Properties and Potential Applications

Thin oxide films have applications in energy conversion, microelectronics and spintronics. Transition metal dopants such as Mn, Fe, Co and Ni have been predicted by DFT to induce magnetic moments in MgO films resulting in dilute magnetic semiconductors [64]. RT ferromagnetism has also been reported for various oxide systems including TiO_2, ZnO and SnO_2 [65]. The most important application is probably related to the catalytic properties of the oxide-metal systems. Most studies involve heterogeneous catalysts consisting of noble metal nanoparticles supported on oxides. The strong metal-support interaction (SMSI) proposed by Tauster et al. [66–68] has stimulated many investigations on the growth of oxide ultrathin films on metal substrates as an inverse catalyst model [18, 36, 47]. These models serve as excellent systems to allow the investigation of oxide-Au interactions and their influence on the catalytic performance.

Recent research demonstrating that the so-called inverse catalysts are reactive or catalytically active themselves has stimulated further interest in these systems. Enhanced catalytic reactivity has been found for CeO_x/Au(111) and TiO_x/Au(111) over Cu(111) and Cu(100) as the typical industrial catalysts towards the water-gas shift reaction [14, 15]. Also, reduced V_2O_3(0001) and V_2O_5(001) films on Au(111) enable oxidation of methanol into formaldehyde and/or methane [52, 69]. STM allows identification of the active sites and research has been conducted into methods for improving the catalytic activity. For example, oxygen vacancies serve as the absorption sites for CO, propane and propene molecules on V_2O_3(0001) and V_2O_5(001) films on Au(111), which can be created by electron irritation of the surface to promote a variety of reactions [51, 70, 71]. CO oxidation that may take

place at the Fe_2O_3/Au and titania/Au perimeter interface can be enhanced by optimization of the coverage of Fe_2O_3 or TiO_x [16, 17].

Thermal programmed desorption (TPD) experiments are usually employed to examine the chemical nature of the desorbing products, providing information on the reaction processes. Figure 5.5 shows the desorption species and their concentration (inserts) after depositing 2-propanol onto the TiO_2/Au(111) and the rutile TiO_2(110) surfaces [72]. The 2-propanol molecules attach to the Ti atoms on both surfaces and desorb at around 300 K. The tail of propanol desorption extends to 560 and 450 K for the TiO_2/Au(111) and the rutile TiO_2(110) surfaces respectively,

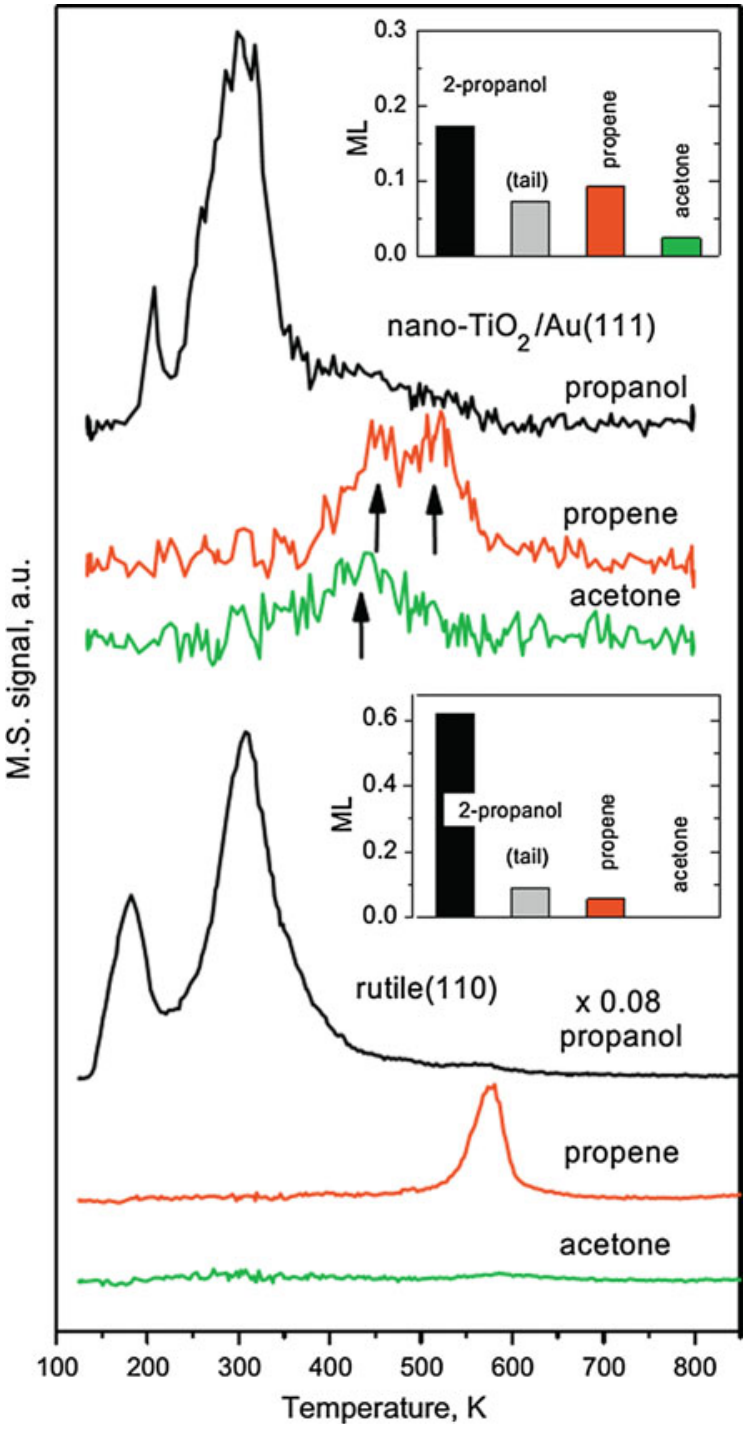

Fig. 5.5 TPD spectra taken from the TiO_2/Au(111) (*top*) and a rutile TiO_2(110) surface (*bottom*) deposited with 2-propanol molecules, showing the traces corresponding to the desorption rate of propanol, propene and acetone. The *inserts* show the distribution of the desorption products referred to the local surface concentration [72]

corresponding to the recombination of surface-bound propoxy and hydrogen. Propene is formed by removing a hydrogen atom from one of the methyl groups of a propoxy species adsorbed on the bridge-bonded oxygen vacancies. Propene desorption has been observed on both TiO_2/Au(111) and the rutile TiO_2(110) surface whereas an additional desorption peak at 450 K appears for the former. This may result from the under-coordinated atoms at the edges of the TiO_2 overlayer in addition to the oxygen vacancy-like defects as the adsorption sites. More importantly, acetone desorption has been observed on the TiO_2/Au(111) surface which was not detected for the rutile TiO_2(110) system. The acetone arises from α-hydride elimination, breaking the oxygen-surface bond and the formation of a double C=O bond. The production of acetone on the TiO_2/Au(111) surface suggests the existence of sites which allow interactions for the α-hydrides. The enhanced reactivity of TiO_2/Au(111) compared with the bulk rutile TiO_2(110) surface may be due to changes in its electronic properties. Despite the picture of active sites and chemical process, many questions remain open, such as the function of Au during the reaction, and how the film-substrate interaction affects the reactivity. Further investigation on the electronic structure may be necessary to uncover the important mechanisms and to provide more information to allow tailoring of the catalytic properties of oxide-Au systems.

Ultrathin films can have crystal structures that are stabilized through the interaction with the substrate and where there are no bulk analogues. This opens the door to the opportunity of fabricating a rich class of oxide surface structures that do not exist in nature. Such novel structures are potentially of great importance in nanoengineering as templates for the self-assembly of adsorbed metal atoms, metal clusters, and molecules. Investigations on the adsorption behavior of metal atoms on ultrathin oxide films include Fe, Au, Pd and Ba on monolayers of MgO, TiO_x, FeO and CeO_x [62, 73–78]. The degree of charge exchange of the metal adsorbates is determined by their electronegativity and plays an important role in the adsorption behavior [62]. For neutral adatoms, e.g. Pd deposited on FeO/Pt(111), random adatom distributions are observed [74]. For the cases where charge transfer takes place, the adatoms tend to form regular arrays and can be either cationic or anionic. For example, electrons are transferred from Au adatoms to the support when deposited on FeO/Pt(111) [74], while conversely the Au adatoms acquire electrons from the support in the MgO/Ag(001) and TiO_x/Pt(111) systems [60, 76]. This charge transfer behavior is illustrated schematically in Fig. 5.6. The oxide film grown on a substrate with high electronegativity donates electrons to the metal substrate (Fig. 5.6a) while the negative charge goes in the opposite direction for the oxide film deposited on the substrate with low electronegativity (Fig. 5.6b). Similar effects come into play when depositing metal adatoms on the supported oxide monolayers. Electronegativity determines the charge state of the metal adatom, its adsorption mode, and it will either reinforce, reduce or even invert the rumpling of the supported oxide films as shown in Figs. 5.6c, d.

The charge transfer behavior is not only determined by the adatom/support species, but is also affected by the coverage of the adatoms. It has recently been reported that structural and electronic characteristics can be controlled by tuning the

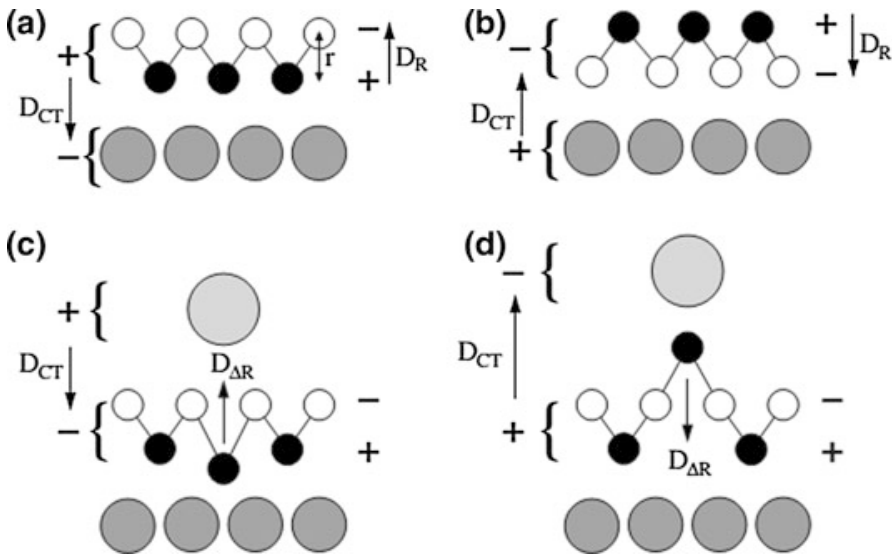

Fig. 5.6 **a** and **b** Sketches showing interfacial charge transfer (D_{CT}) and the film rumpling (D_R) dipole moments for an oxide monolayer (*small black circles* represent cations, *white circles* represent anions) grown on a metal substrate (*large grey circles*). Depending on the electronegativity of the substrate, charge can transfer from (**a**) or into (**b**) the film. The adatom can either (**c**) adsorb directly on the oxide surface, resulting in increased separation of the anion-cation planes, i.e. reinforce the rumpling, or (**d**) locally reduce or even invert the rumpling. Such structural changes are driven by charge transfer between the adatom and the support [62]

Ba deposition on Ti_2O_3 monolayers grown on Au(111) [78]. Figure 5.7 shows the evolution of Ba adsorption on Ti_2O_3/Au(111) with the Ba coverage increased from 0.07 to 0.62 ML. For low Ba doses (0.07 ML), the adatoms are randomly distributed, and have as their adsorption site the hollow location of the honeycomb Ti_2O_3 lattice (Fig. 5.7, 0.07 ML). Two well-ordered surface structures are generated at coverages of 1/3 and 2/3 ML. The 1/3 ML order arises when the Ba adatoms fill the six second nearest neighbor hollow sites (Fig. 5.7, 0.35 ML), whereas the 2/3 ML ordering occurs when the three first nearest hollow sites are occupied (Fig. 5.7, 0.62 ML). A labyrinth-like phase is observed for Ba coverages between 1/3 and 2/3 ML (Fig. 5.7, 0.43, 0.49 ML). The structural configurations are determined by Ba–Ba repulsion through dipole-dipole interactions induced by charge transfer. The overall charge transfer from Ba to the Au substrate increases with raised Ba dose, which also results in steadily increased Ti_2O_3 film rumpling and a decreased Au work function. The findings that the adsorption behavior can be tuned by choosing the combination of metal adatom species and the oxide thin film, as well as varying the adatom coverage, open up the possibility of designing metal-oxide interfaces with specific and novel properties.

Molecular self-assembly is another important area of nanostructure engineering where the surface structure of the substrate has a significant influence. For trimethyl acetic acid (TMAA) on the pinwheel reconstructions of TiO/Au(111), the molecules preferentially occupy sites near the centers of the pinwheels as shown in Fig. 5.8a [56]. With increased coverage, the adsorption pattern evolves into a triad

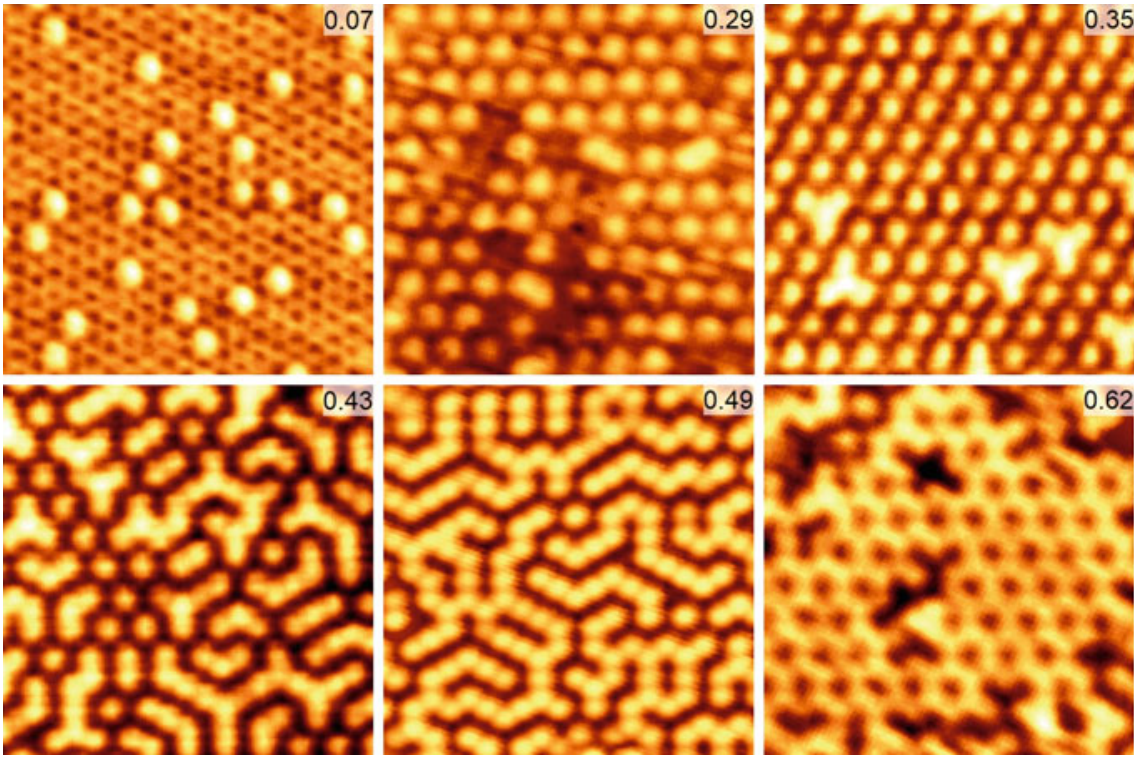

Fig. 5.7 STM images showing the Ba adsorption on the honeycomb Ti_2O_3 monolayer grown on Au(111). The Ba coverage is determined as 0.07, 0.29, 0.35, 0.43, 0.49 and 0.62 ML as indicated on each image. (Image sizes: 10 × 10 nm^2; V_s = 0.35–1.00 V; I_t = 0.18–0.28 nA) [78]

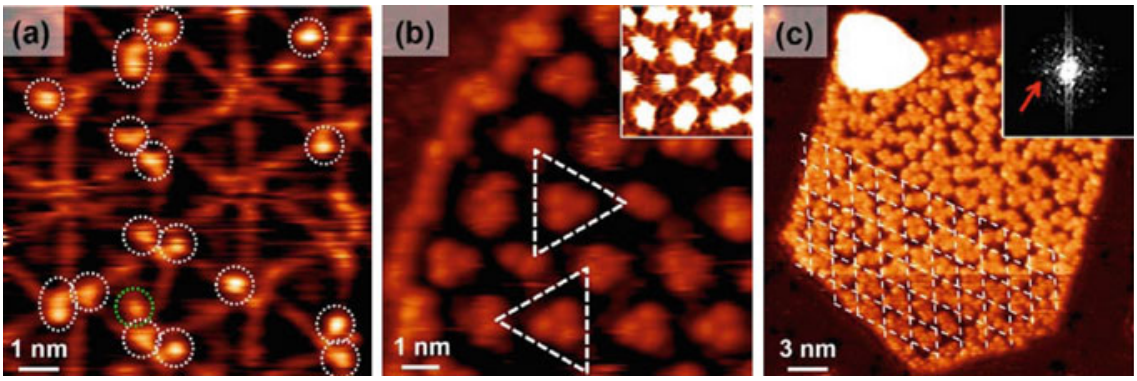

Fig. 5.8 Adsorption of TMAA on the pinwheel TiO/Au(111) surface at coverages of **a** 0.02 ML, **b** 0.06 ML and **c** 0.15 ML [56]

with three-fold symmetry (Fig. 5.8b). Further increasing the TMAA dose gives rise to an extended molecular network that avoids the sites at the centers of the triangles of the pinwheels (Fig. 5.8c). Apart from the pinwheel TiO/Au(111) system, many other ultrathin film structures may serve as templates for substrate-directed molecular self-assembly. Potential candidates include the honeycomb Ti_2O_3/Au (111) surface with hollow sites and the rectangular-like phases with gaps between the row structures. The richness of the various oxide structures on Au(111) provides a progressive step towards molecular engineering on the nanoscale.

5.6 Conclusions and Perspectives

This chapter has explored the rich variety of structures and properties observed in ultrathin oxide films on Au(111) surfaces. The ultrathin film structures may be divided into two categories, namely those which follow the hexagonal symmetry of the substrate and those that have row structures with rectangular-like surface unit cells. Multiple factors determine the surface structure of the oxide layers among which stoichiometry and substrate-film lattice mismatch tend to dominate. These factors can be controlled by selecting combinations of oxide and substrate materials, as well as optimizing the growth conditions such as the growth temperature, oxidation environment, post-process annealing steps and film thickness. The development of a comprehensive understanding of all the aspects that determine the film growth and properties will enable the future fabrication of precisely controlled oxide thin films. This is one of the critical materials challenges for nano-engineering of oxides.

References

1. Motoyama Y, Matsuzaki H, Murakami H (2001) A study of the secondary electron yield gamma of insulator cathodes for plasma display panels. IEEE Trans Electron Dev 48(8):1568–1574. doi:10.1109/16.936562
2. Matulevich YT, Vink TJ, van Emmichoven PAZ (2002) Low-energy ion-induced electron emission from a MgO(100) thin film: The role of the MgO-substrate interface. Phys Rev Lett 89(16):167601. doi:10.1103/PhysRevLett.89.167601
3. Shaikhutdinov S, Freund HJ (2012) Ultrathin oxide films on metal supports: structure-reactivity relations. Annu Rev Phys Chem 63:619–633. doi:10.1146/annurev-physchem-032511-143737
4. Chambers SA (2000) Epitaxial growth and properties of thin film oxides. Surf Sci Rep 39(5–6):105–180. doi:10.1016/s0167-5729(00)00005-4
5. Nilius N (2009) Properties of oxide thin films and their adsorption behavior studied by scanning tunneling microscopy and conductance spectroscopy. Surf Sci Rep 64(12):595–659. doi:10.1016/j.surfrep.2009.07.004
6. Goniakowski J, Finocchi F, Noguera C (2008) Polarity of oxide surfaces and nanostructures. Rep Prog Phys 71(1):55. doi:10.1088/0034-4885/71/1/016501
7. Huber H, McIntosh D, Ozin GA (1977) Metal atom model for oxidation of carbon-monoxide to carbon-dioxide-gold atom carbon monoxide dioxygen reaction and gold atom carbon dioxide reaction. Inorg Chem 16(5):975–979. doi:10.1021/ic50171a001
8. Green IX, Tang WJ, Neurock M, Yates JT (2011) Spectroscopic observation of dual catalytic sites during oxidation of CO on a Au/TiO_2 catalyst. Science 333(6043):736–739. doi:10.1126/science.1207272
9. Fu Q, Saltsburg H, Flytzani-Stephanopoulos M (2003) Active nonmetallic Au and Pt species on ceria-based water-gas shift catalysts. Science 301(5635):935–938. doi:10.1126/science.1085721
10. Fu Q, Weber A, Flytzani-Stephanopoulos M (2001) Nanostructured Au-CeO_2 catalysts for low-temperature water-gas shift. Catal Lett 77(1–3):87–95. doi:10.1023/a:1012666128812
11. Ueda A, Oshima T, Haruta M (1997) Reduction of nitrogen monoxide with propene in the presence of oxygen and moisture over gold supported on metal oxides. Applied Catalysis B-Environmental 12(2–3):81–93. doi:10.1016/s0926-3373(96)00069-0

12. Zheng N, Stucky GD (2006) A general synthetic strategy for oxide-supported metal nanoparticle catalysts. J Am Chem Soc 128(44):14278–14280. doi:10.1021/ja0659929
13. Hayashi T, Tanaka K, Haruta M (1998) Selective vapor-phase epoxidation of propylene over Au/TiO_2 catalysts in the presence of oxygen and hydrogen. J Catal 178(2):566–575. doi:10.1006/jcat.1998.2157
14. Rodriguez JA, Ma S, Liu P, Hrbek J, Evans J, Perez M (2007) Activity of CeO_x and TiO_x nanoparticles grown on Au(111) in the water-gas shift reaction. Science 318(5857):1757–1760. doi:10.1126/science.1150038
15. Senanayake SD, Stacchiola D, Evans J, Estrella M, Barrio L, Pérez M, Hrbek J, Rodriguez JA (2010) Probing the reaction intermediates for the water–gas shift over inverse CeO_x/Au(111) catalysts. J Catal 271(2):392–400. doi:10.1016/j.jcat.2010.02.024
16. Yan T, Redman DW, Yu W-Y, Flaherty DW, Rodriguez JA, Mullins CB (2012) CO oxidation on inverse Fe_2O_3/Au(111) model catalysts. J Catal 294:216–222. doi:10.1016/j.jcat.2012.07.024
17. Magkoev TT (2007) Interaction of carbon monoxide and oxygen at the surface of inverse titania/Au model catalyst. Surf Sci 601(14):3143–3148. doi:10.1016/j.susc.2007.05.015
18. Wu C, Marshall MSJ, Castell MR (2011) Surface structures of ultrathin TiO_x films on Au (111). J Phys Chem C 115(17):8643–8652. doi:10.1021/jp111385n
19. Pan Y, Benedetti S, Nilius N, Freund H-J (2011) Change of the surface electronic structure of Au(111) by a monolayer MgO(001) film. Phys Rev B 84(7):075456. doi:10.1103/PhysRevB.84.075456
20. Guimond S, Goebke D, Romanyshyn Y, Sturm JM, Naschitzki M, Kuhlenbeck H, Freund H-J (2008) Growth and characterization of ultrathin V_2O_y (y approximate to 5) films on Au(111). J Phys Chem C 112(32):12363–12373. doi:10.1021/jp8011365
21. Guimond S, Sturm JM, Goebke D, Romanyshyn Y, Naschitzki M, Kuhlenbeck H, Freund H-J (2008) Well-ordered V_2O_5(001) thin films on Au(111): growth and thermal stability. J Phys Chem C 112(31):11835–11846. doi:10.1021/jp8011156
22. Deng X, Matranga C (2009) Selective growth of Fe_2O_3 nanoparticles and islands on Au(111). J Phys Chem C 113(25):11104–11109. doi:10.1021/jp9021954
23. Potapenko DV, Hrbek J, Osgood RM (2008) Scanning tunneling microscopy study of titanium oxide nanocrystals prepared on Au(111) by reactive-layer-assisted deposition. ACS Nano 2 (7):1353–1362. doi:10.1021/nn800169y
24. Song D, Hrbek J, Osgood R (2005) Formation of TiO_2 nanoparticles by reactive-layer-assisted deposition and characterization by XPS and STM. Nano Lett 5(7):1327–1332. doi:10.1021/nl0505703
25. Ma S, Rodriguez J, Hrbek J (2008) STM study of the growth of cerium oxide nanoparticles on Au(111). Surf Sci 602(21):3272–3278. doi:10.1016/j.susc.2008.08.021
26. Potapenko DV, Osgood RM (2009) Preparation of TiO_2 nanocrystallites by oxidation of Ti-Au(111) surface alloy. Nano Lett 9(6):2378–2383. doi:10.1021/nl900904s
27. Ragazzon D, Schaefer A, Farstad MH, Walle LE, Palmgren P, Borg A, Uvdal P, Sandell A (2013) Chemical vapor deposition of ordered TiO_x nanostructures on Au(111). Surf Sci 617:211–217. doi:10.1016/j.susc.2013.07.019
28. Biener MM, Friend CM (2004) Heteroepitaxial growth of novel MoO_3 nanostructures on Au (111). Surf Sci 559(2–3):L173–L179. doi:10.1016/j.susc.2004.01.021
29. Fu Q, Wagner T (2007) Interaction of nanostructured metal overlayers with oxide surfaces. Surf Sci Rep 62(11):431–498. doi:10.1016/j.surfrep.2007.07.001
30. Bach CE, Giesen M, Ibach H, Einstein TL (1997) Stress relief in reconstruction. Phys Rev Lett 78(22):4225–4228. doi:10.1103/PhysRevLett.78.4225
31. Barth JV, Brune H, Ertl G, Behm RJ (1990) Scanning tunneling microscopy observations on the reconstructed Au(111) surface-atomic-structure, long-range superatructure, rotational domains, and surface-defects. Physical Review B 42(15):9307–9318. doi:10.1103/PhysRevB.42.9307

32. Lauritsen JV, Besenbacher F (2006) Model catalyst surfaces investigated by scanning tunneling microscopy. In: Gates BC, Knozinger H (eds) Advances in catalysis, vol 50. Advances in catalysis. Elsevier Academic Press Inc, San Diego, pp 97–147. doi:10.1016/s0360-0564(06)50003-3
33. Morgenstern K, Kibsgaard J, Lauritsen JV, Laegsgaard E, Besenbacher F (2007) Cobalt growth on two related close-packed noble metal surfaces. Surf Sci 601(9):1967–1972. doi:10.1016/j.susc.2007.02.018
34. Khan NA, Matranga C (2008) Nucleation and growth of Fe and FeO nanoparticles and films on Au(111). Surf Sci 602(4):932–942. doi:10.1016/j.susc.2007.12.027
35. Window AJ, Hentz A, Sheppard DC, Parkinson GS, Woodruff DP, Unterberger W, Noakes TCQ, Bailey P, Ganduglia-Pirovano MV, Sauer J (2012) The structure of epitaxial V_2O_3 films and their surfaces: a medium energy ion scattering study. Surf Sci 606(21–22):1716–1727. doi:10.1016/j.susc.2012.07.015
36. Seifert J, Meyer E, Winter H, Kuhlenbeck H (2012) Surface termination of an ultrathin V_2O_3-film on Au(111) studied via ion beam triangulation. Surf Sci 606(9–10):L41–L44. doi:10.1016/j.susc.2012.02.004
37. Dupuis AC, Abu Haija M, Richter B, Kuhlenbeck H, Freund HJ (2003) V_2O_3(0001) on Au(111) and W(110): growth, termination and electronic structure. Surf Sci 539(1–3):99–112. doi:10.1016/s0039-6028(03)00752-0
38. Window AJ, Hentz A, Sheppard DC, Parkinson GS, Niehus H, Ahlbehrendt D, Noakes TCQ, Bailey P, Woodruff DP (2011) V_2O_3(0001) surface termination: Phase equilibrium. Phys Rev Lett 107(1):016105. doi:10.1103/PhysRevLett.107.016105
39. Li M, Altman EI (2014) Cluster-size dependent phase transition of Co oxides on Au(111). Surf Sci 619:L6–L10. doi:10.1016/j.susc.2013.09.029
40. Sindhu S, Heiler M, Schindler KM, Neddermeyer H (2003) A photoemission study of CoO-films on Au(111). Surf Sci 541(1–3):197–206. doi:10.1016/s0039-6028(03)00917-8
41. Li M, Altman EI (2014) Shape, morphology, and phase transitions during Co oxide growth on Au(111). J Phys Chem C 118(24):12706–12716. doi:10.1021/jp411375w
42. Biener MM, Biener J, Schalek R, Friend CM (2004) Growth of nanocrystalline MoO_3 on Au (111) studied by in situ scanning tunneling microscopy. J Chem Phys 121(23):12010–12016. doi:10.1063/1.1808422
43. Guimond S, Göbke D, Sturm JM, Romanyshyn Y, Kuhlenbeck H, Cavalleri M, Freund HJ (2013) Well-ordered molybdenum oxide layers on Au(111): preparation and properties. J Phys Chem C 117(17):8746–8757. doi:10.1021/jp3113792
44. Pan Y, Benedetti S, Noguera C, Giordano L, Goniakowski J, Nilius N (2012) Compensating edge polarity: A means to alter the growth orientation of MgO nanostructures on Au(111). J Phys Chem C 116(20):11126–11132. doi:10.1021/jp302302v
45. Benedetti S, Nilius N, Torelli P, Renaud G, Freund HJ, Valeri S (2011) Competition between polar and nonpolar growth of MgO thin films on Au(111). J Phys Chem C 115(46):23043–23049. doi:10.1021/jp207901a
46. Nilius N, Benedetti S, Pan Y, Myrach P, Noguera C, Giordano L, Goniakowski J (2012) Electronic and electrostatic properties of polar oxide nanostructures: MgO(111) islands on Au (111). Phys Rev B 86(20):205410. doi:10.1103/PhysRevB.86.205410
47. Stavale F, Pascua L, Nilius N, Freund H-J (2013) Morphology and luminescence of ZnO films grown on a Au(111) support. J Phys Chem C 117(20):10552–10557. doi:10.1021/jp401939x
48. Wu C, Castell MR (2012) Ba and BaO_x surface structures on Au(111). Surf Sci 606(3–4):181–185. doi:10.1016/j.susc.2011.09.013
49. Quek SY, Biener MM, Biener J, Friend CM, Kaxiras E (2005) Tuning electronic properties of novel metal oxide nanocrystals using interface interactions: MoO_3 monolayers on Au(111). Surf Sci 577(2–3):L71–L77. doi:10.1016/j.susc.2005.01.012
50. Deng X, Yao K, Sun K, Li W, Lee J, Matranga C (2013) Growth of single- and bilayer ZnO on Au(111) and interaction with copper. J Phys Chem C 117(21):11211–11218. doi:10.1021/jp402008w

51. Kuhlenbeck H, Shaikhutdinov S, Freund HJ (2013) Well-ordered transition metal oxide layers in model catalysis–a series of case studies. Chem Rev 113(6):3986–4034. doi:10.1021/cr300312n
52. Romanyshyn Y, Guimond S, Gobke D, Sturm JM, Kuhlenbeck H, Dobler J, Ganduglia-Pirovano MV, Sauer J, Freund HJ (2011) Methanol adsorption on V_2O_3(0001). Top Catal 54(10–12):669–684. doi:10.1007/s11244-011-9685-y
53. Simic-Milosevic V, Nilius N, Rust HP, Freund HJ (2008) Local band gap modulations in non-stoichiometric V_2O_3 films probed by scanning tunneling spectroscopy. Phys Rev B 77(12):125112. doi:10.1103/PhysRevB.77.125112
54. Feiten FE, Seifert J, Paier J, Kuhlenbeck H, Winter H, Sauer J, Freund H-J (2015) Surface Structure of V_2O_3(0001) Revisited. Phys Rev Lett 114(21). doi:10.1103/PhysRevLett.114.216101
55. Guimond S, Abu Haija M, Kaya S, Lu J, Weissenrieder J, Shaikhutdinov S, Kuhlenbeck H, Freund HJ, Dobler J, Sauer J (2006) Vanadium oxide surfaces and supported vanadium oxide nanoparticles. Top Catal 38(1–3):117–125. doi:10.1007/s11244-006-0076-8
56. Li ZS, Potapenko DV, Osgood RM (2014) Using moire patterning to map surface reactivity versus atom registration: Chemisorbed trimethyl acetic acid on TiO/Au(111). J Phys Chem C 118(51):29999–30005. doi:10.1021/jp5103302
57. Bouzidi L, Slavin AJ (2005) Ultrathin films of lead oxide on gold: dependence of stoichiometry, stability and thickness on O_2 pressure and annealing temperature. Surf Sci 580(1–3):195–206. doi:10.1016/j.susc.2005.01.056
58. Barcaro G, Cavaliere E, Artiglia L, Sementa L, Gavioli L, Granozzi G, Fortunelli A (2012) Building principles and structural motifs in TiOx ultrathin films on a (111) substrate. J Phys Chem C 116(24):13302–13306. doi:10.1021/jp303730j
59. Tung RT (2001) Recent advances in Schottky barrier concepts. Mater Sci Eng R-Reports 35(1–3):1–138. doi:10.1016/s0927-796x(01)00037-7
60. Giordano L, Cinquini F, Pacchioni G (2006) Tuning the surface metal work function by deposition of ultrathin oxide films: density functional calculations. Phys Rev B 73(4):045414. doi:10.1103/PhysRevB.73.045414
61. Goniakowski J, Giordano L, Noguera C (2010) Polarity of ultrathin MgO(111) films deposited on a metal substrate. Phys Rev B 81(20):205404. doi:10.1103/PhysRevB.81.205404
62. Goniakowski J, Noguera C, Giordano L, Pacchioni G (2009) Adsorption of metal adatoms on FeO(111) and MgO(111) monolayers: effects of charge state of adsorbate on rumpling of supported oxide film. Phys Rev B 80(12):125403. doi:10.1103/PhysRevB.80.125403
63. Song Z, Cai TH, Chang ZP, Liu G, Rodriguez JA, Hrbek J (2003) Molecular level study of the formation and the spread of MoO_3 on Au (111) by scanning tunneling microscopy and X-ray photoelectron spectroscopy. J Am Chem Soc 125(26):8059–8066. doi:10.1021/ja034862m
64. Wu P, Cao G, Tang F, Huang M (2014) Electronic and magnetic properties of transition metal doped MgO sheet: a density-functional study. Comput Mater Sci 86:180–185. doi:10.1016/j.commatsci.2014.01.052
65. Coey JMD (2006) Dilute magnetic oxides. Curr Opin Solid State Mater Sci 10(2):83–92. doi:10.1016/j.cossms.2006.12.002
66. Tauster SJ, Fung SC, Garten RL (1978) Strong metal-support interactions-group-8 noble-metals supported on TiO_2. J Am Chem Soc 100(1):170–175. doi:10.1021/ja00469a029
67. Tauster SJ, Fung SC, Baker RTK, Horsley JA (1981) Strong-interactions in supported-metal catalysts. Science 211(4487):1121–1125. doi:10.1126/science.211.4487.1121
68. Tauster SJ (1987) Strong metal-support interactions. Acc Chem Res 20(11):389–394. doi:10.1021/ar00143a001
69. Sturm JM, Goebke D, Kuhlenbeck H, Doebler J, Reinhardt U, Ganduglia-Pirovano MV, Sauer J, Freund HJ (2009) Partial oxidation of methanol on well-ordered V_2O_5(001)/Au(111) thin films. Phys Chem Chem Phys 11(17):3290–3299. doi:10.1039/b822384j
70. Abu Haija M, Guimond S, Uhl A, Kuhlenbeck H, Freund HJ (2006) Adsorption of water on thin V_2O_3(0001) films. Surf Sci 600(5):1040–1047. doi:10.1016/j.susc.2005.12.035

71. Bandara A, Abu-Haija M, Höbel F, Kuhlenbeck H, Rupprechter G, Freund H-J (2007) Molecular adsorption on V_2O_3(0001)/Au(111) surfaces. Top Catal 46(1–2):223–230. doi:10.1007/s11244-007-0332-6
72. Potapenko DV, Li Z, Lou Y, Guo Y, Osgood RM (2013) 2-Propanol reactivity on in situ prepared Au(111)-supported TiO_2 nanocrystals. J Catal 297:281–288. doi:10.1016/j.jcat.2012.10.020
73. Barcaro G, Fortunelli A (2009) Adsorption and Diffusion of Fe on a Titania Ultrathin Film. J Phys Chem A 113(52):14860–14866. doi:10.1021/jp904998c
74. Giordano L, Pacchioni G, Goniakowski J, Nilius N, Rienks EDL, Freund H-J (2008) Charging of metal adatoms on ultrathin oxide films: Au and Pd on FeO/Pt(111). Phys Rev Lett 101(2):026102. doi:10.1103/PhysRevLett.101.026102
75. Cavaliere E, Kholmanov I, Gavioli L, Sedona F, Agnoli S, Granozzi G, Barcaro G, Fortunelli A (2009) Directed assembly of Au and Fe nanoparticles on a TiO_x/Pt(111) ultrathin template: the role of oxygen affinity. Phys Chem Chem Phys 11(47):11305–11309. doi:10.1039/b915641k
76. Barcaro G, Fortunelli A, Granozzi G (2008) Metal adsorption on oxide polar ultrathin films. Phys Chem Chem Phys 10(14):1876–1882. doi:10.1039/b719346g
77. Baron M, Bondarchuk O, Stacchiola D, Shaikhutdinov S, Freund HJ (2009) Interaction of gold with cerium oxide supports: CeO_2(111) thin films vs CeOx nanoparticles. J Phys Chem C 113(15):6042–6049. doi:10.1021/jp9001753
78. Wu C, Castell MR, Goniakowski J, Noguera C (2015) Stoichiometry engineering of ternary oxide ultrathin films: $Ba_xTi_2O_3$ on Au(111). Phys Rev B 91(15):155424. doi:10.1103/PhysRevB.91.155424